J Biomol NMR (2010) 47:7–17
DOI 10.1007/s10858-010-9406-z

ARTICLE

Broadband ^{15}N–^{13}C dipolar recoupling via symmetry-based RF pulse schemes at high MAS frequencies

Christian Herbst · Jirada Herbst · Michela Carella · Jörg Leppert · Oliver Ohlenschläger · Matthias Görlach · Ramadurai Ramachandran

Received: 14 December 2009 / Accepted: 23 February 2010 / Published online: 20 March 2010

Abstract An approach for generating efficient $RN_n^{\nu_S,\nu_k}$ symmetry-based dual channel RF pulse schemes for γ-encoded broadband ^{15}N–^{13}C dipolar recoupling at high magic angle spinning frequencies is presented. The method involves the numerical optimisation of the RF phase-modulation profile of the basic "*R*" element so as to obtain heteronuclear double quantum dipolar recoupling sequences with satisfactory magnetisation transfer characteristics. The basic "*R*" element was implemented as a sandwich of a small number of short pulses of equal duration with each pulse characterised by a RF phase and amplitude values. The performance characteristics of the sequences were evaluated via numerical simulations and ^{15}N–^{13}C chemical shift correlation experiments. Employing such ^{13}C–^{15}N double-quantum recoupling sequences and the multiple receiver capabilities available in the current generation of NMR spectrometers, the possibility to simultaneously acquire 3D NCC and CNH chemical shift correlation spectra is also demonstrated.

Keywords MAS · Solid state NMR · Chemical shift correlation · Symmetry-based RF pulse schemes · Multiple Receivers · RNA

Introduction

Mixing schemes leading to homo- and heteronuclear dipolar coupling mediated coherence transfers form an important building block of several RF pulse sequences that are employed in the magic-angle spinning solid state NMR studies of biological systems such as proteins and RNAs. For example, ^{15}N–^{13}C and ^{15}N–^{13}C–^{13}C chemical shift correlation experiments involving ^{15}N–^{13}C dipolar recoupling are used for the assignment of ^{15}N and ^{13}C resonances in peptides, proteins and RNAs (Sun et al. 1997; Hong 1999; Rienstra et al. 2000; Pauli et al. 2001; Detken et al. 2001; Castellani et al. 2003; van Rossum et al. 2003; Riedel et al. 2005; Frericks et al. 2006; Siemer et al. 2006; Kehlet et al. 2007; Hansen et al. 2007). Possibilities for obtaining proton assignments in fully protonated proteins via CANH, CONH and NCAH experiments using direct proton detection at fast MAS have been demonstrated recently (Zhou et al. 2007a). Coupled with empirical backbone dihedral angles that can be obtained from ^{13}C isotropic chemical shifts, ^{1}H–^{1}H distance restraints obtained via the 3D CON(H)H experiment have been successfully employed for obtaining the high resolution structure of the $\beta 1$ immunoglobulin binding domain of protein G (GB1) that was uniformly labelled with ^{13}C, ^{15}N and ^{2}H nuclei and then back-exchanged with H_2O (Zhou et al. 2007b). Experiments involving the evolution of ^{13}C–^{15}N heteronuclear double-quantum coherences, either under the influence of the CSAs of the coupled nuclei or heteronuclear dipolar couplings with the directly attached

Electronic supplementary material The online version of this article (doi:10.1007/s10858-010-9406-z) contains supplementary material, which is available to authorized users.

C. Herbst · J. Herbst · M. Carella · J. Leppert · O. Ohlenschläger · M. Görlach · R. Ramachandran (✉)
Research Group Biomolecular NMR Spectroscopy, Leibniz Institute for Age Research, Fritz Lipmann Institute, 07745 Jena, Germany
e-mail: raman@fli-leibniz.de

J. Herbst
Department of Mathematics, Statistics and Computer, Faculty of Science, Ubon Ratchathani University, Ubon Ratchathani 34190, Thailand

protons, have permitted the extraction of torsion angle constraints in proteins. Although weak dipolar couplings between low γ nuclei such as ^{15}N and ^{13}C are generally lost under MAS, it is possible to inhibit the spatial averaging of these couplings (Bennett et al. 1994; Griffin 1998; Dusold and Sebald 2000; Baldus 2002). Levitt et al. (2002) have developed an elegant symmetry-based approach that provides a convenient platform for designing efficient RF pulse schemes for the recoupling and decoupling of different anisotropic nuclear spin interactions in rotating solids. Symmetry-based RF pulse sequences, in general, have found diverse applications in MAS NMR studies of biological systems. Two classes of symmetry-based sequences, denoted as CN_n^v and RN_n^v, have been developed till date. The CN_n^v class of RF pulse schemes involves the application of a basic element "C" corresponding to an RF cycle with unity propagator $U_{RF}(t_c) = \pm 1$. N such cycles are applied over n rotor periods τ_r with successive C elements incremented in phase by $v2\pi/N$. RF pulse sequences belonging to RN_n^v symmetry involve the application of the pulse sandwich $\{R_\phi R_{-\phi}\}$, corresponding to a propagator $U_{RF} = \exp(-i4\phi I_z)$, where $\phi = \pi v/N$ and R is typically a pulse that rotates the nuclear spins through 180° about the x-axis. The pulse sandwich $\{R_\phi R_{-\phi}\}$ is repeated $N/2$ times over n rotor periods so as to form an RF cycle with unity propagator $U_{RF}(t_c) = \pm 1$. N, n and v are all integers and appropriate values for these are chosen, via the selection rule for CN_n^v and RN_n^v symmetry, to generate the desired average Hamiltonian. Recoupling of heteronuclear dipolar interactions leading to polarization transfer is of interest in this study and this can be achieved via four different symmetry classes, denoted as $CN_n^{v_S,v_K}$, $CRN_n^{v_S,v_K}$, $RCN_n^{v_S,v_K}$ and $RN_n^{v_S,v_K}$, that require the simultaneous application of RF fields at the Larmor frequencies of the two spins 'S' and 'K' involved. The phase incrementation for the S-spin irradiation follows the above mentioned construction rule for C-sequences (in the case of $CN_n^{v_S,v_K}$ or $CRN_n^{v_S,v_K}$) or for R-sequences (in the case of $RCN_n^{v_S,v_K}$ or $RN_n^{v_S,v_K}$) and depends on the symmetry numbers N, n and v_s. Similarly, the phase incrementation for the K-spin irradiation follows the construction rule for C-sequences (in the case of $CN_n^{v_S,v_K}$ or $RCN_n^{v_S,v_K}$) or for R-sequences (in the case of $CRN_n^{v_S,v_K}$ or $RN_n^{v_S,v_K}$) and depends on the symmetry numbers N, n and v_k (Levitt 2002). The selection rules for dual channel sequences have been derived (Brinkmann and Levitt 2001) and a variety of inequivalent $RN_n^{v_S,v_K}$ and $CRN_n^{v_S,v_K}$ sequences have been reported for achieving γ-encoded heteronuclear double-quantum recoupling, with suppression of all chemical shift anisotropies and homonuclear dipolar coupling terms. The performance of the symmetry-based sequences critically depends on the choice of the basic element and, typically, good candidate sequences are identified via a combinatorial approach involving an assessment of the performance of different inequivalent sequences using a variety of composite pulse based basic elements. Employing such an approach, Brinkmann and Levitt have shown that the symmetries $R22_7^{9,6}$, $R24_9^{8,7}$ and $R24_9^{-5,-10}$, together with the corresponding R elements $\{(\pi/2)_\pi(2\pi)_0(\pi)_\pi(\pi/2)_0\}^{s,k}$, $\{(\pi/2)_\pi(2\pi)_0(\pi)_\pi(\pi/2)_0\}^{s,k}$ and $\{(\pi/3)_0(5\pi/3)_\pi(\pi/3)_0\}^{s,k}$, lead to satisfactory broadband ^{13}C–^{15}N double-quantum recoupling. However, it is conceivable that the RF pulse schemes identified via the combinatorial approach need not necessarily represent the best possible solutions that can be generated for achieving dipolar recoupling. In addition, due to the dependence of the RF field strength requirements on the spinning speed employed, it may be even difficult to implement symmetry-based dipolar recoupling schemes based on conventional composite RF pulses, such as those mentioned above, in certain spinning speed regimes. With such sequences, the RF field strength requirements could become either too large that is beyond the hardware limits of the spectrometer system or could lead to substantial signal losses due to interference between the decoupling and recoupling RF fields (Bennett et al. 1998). It is worth mentioning that in MAS solid state NMR based structural studies of biomolecular systems it is advantageous to employ high Zeeman fields for obtaining improved sensitivity and resolution. On the other hand, the effects of CSA also increase with higher Zeeman field strength employed and this typically makes it necessary to carry out the experiments at high MAS frequencies to minimise spinning sideband intensities. High MAS frequencies are also useful for generating chemical shift correlation spectra via direct ^{1}H detection. Hence, methods that facilitate the design of efficient dipolar recoupling schemes for applications at high MAS frequencies are of great interest in biomolecular NMR studies. Motivated by these factors, we have been examining recently an alternative approach for designing efficient symmetry-based dipolar recoupling schemes (Herbst et al. 2009a, b, c). In this approach, symmetries that would potentially lead to satisfactory solutions are first identified taking into consideration the MAS frequency to be employed and the available/applicable RF power. In the second step, phase/amplitude modulated 180°/360° RF pulses with appropriate duration, as determined by the symmetry and MAS frequency, were generated considering a simple spin-1/2 system and different inversion/null-rotation bandwidths. In the final step, these pulses were used as the starting point for the numerical optimisation to generate RF pulse sequences with satisfactory magnetisation transfer characteristics over the required range of resonance offsets and RF field inhomogeneities. Such an approach was successfully adopted in the design of CN_n^v and RN_n^v symmetry-based pulse schemes for generating ^{13}C–^{13}C dipolar and scalar coupling mediated chemical shift correlation spectra

at high MAS frequencies. The efficacy of this approach for the design of broadband $RN_n^{\nu_S,\nu_k}$ symmetry-based pulse schemes for γ-encoded ^{15}N–^{13}C double quantum dipolar recoupling is demonstrated here via numerical simulations and experimental measurements. Employing symmetry-based ^{13}C–^{15}N double-quantum recoupling sequences and the multiple receiver capabilities available in the current generation of NMR spectrometers, the possibility to simultaneously acquire 3D NCC and CNH chemical shift correlation spectra is also demonstrated.

Numerical and experimental procedures

^{15}N–^{13}C dipolar recoupling sequences were generated at a few representative MAS frequencies considering simultaneous application of ^{1}H decoupling during mixing, unless mentioned otherwise. Phase modulated 180° RF pulses of constant amplitude were employed in this study as the basic R elements and were generated via the global optimisation procedure "genetic algorithms" (GA) (Goldberg 1989; Forrest 1993; Judson 1997; Haupt and Haupt 2004; Freeman and Wu 1987; Wu and Freeman 1989; Xu et al. 1992; Herbst et al. 2009a, b, c). The GA program package GAlib (Wall 1996), as employed in our recent study (Herbst et al. 2009a, b, c), was used. Typically, a population size and number of generations of 500 were used in the GA calculations. The pulses were implemented as a sandwich of a small number of pulses of equal duration, typically in the range of 1.5–3.0 μs, and were generated employing RF field strengths in the range of 15–45 kHz. The GA derived pulses, with inversion bandwidths in the range of 8–20 kHz, were generally constructed such that the RF phase modulation profiles are symmetric with respect to the center of the pulse and were used as the starting basic R element in implementing $RN_n^{\nu_S,\nu_k}$ symmetry-based pulse schemes. In addition to the inequivalent $RN_n^{\nu_S,\nu_k}$ sequences with $N \leq 24$, $n \leq 9$ and $N/n \leq 7$ that have been reported by Brinkmann and Levitt (2001) for achieving γ-encoded heteronuclear double-quantum recoupling, new sequences with $N \leq 24$ and $n > 9$ and with the same symmetry-allowed terms as in the study of Brinkmann and Levitt [$(m, \mu_s, \mu_k) = (1, -1, -1), (-1, 1, 1)$] were also generated (see supplementary material) based on the selection rules for dual channel pulse schemes. At a given MAS frequency, only those symmetries were considered for which phase-modulated basic R elements of required durations can be generated employing the available/applicable RF power. The phase modulation profiles of the basic elements were subsequently optimised considering a two spin ^{15}N–^{13}C system via the nonlinear least-squares optimisation procedure NL2SOL implemented in the SPINEVOLUTION program (Veshtort and Griffin 2006) so as to achieve, over the resonance offset range of the ^{15}N and ^{13}C nuclei, the best possible performance of the symmetry-based scheme. Considering that the initial rate of transfer of magnetisation from one spin to another is a measure of the efficacy of the mixing sequence, with a faster transfer representing an efficient dipolar recoupling, optimised RF pulse schemes were obtained in this study by monitoring the magnitude of longitudinal magnetisation transferred to the carbon spin ($I_{sz} \rightarrow -I_{kz}$) as a function of the mixing time, starting with z magnetisation on the carbon spin at zero mixing time. Considering that in a simple system of directly coupled ^{15}N and ^{13}C nuclei it is possible to transfer magnetisation from one spin to another in a relatively short period of $\sim$2–3 ms, DQ dipolar recoupling sequences were developed in this study by maximising the magnitude of the longitudinal magnetisation transferred to the ^{15}N spin at $\sim$2 ms. Typically, a resonance offset range of ±5 kHz for ^{13}C and either ±5 or ±1 kHz for ^{15}N were employed with different CSA values for the two nuclei. The local optimisation run was repeated several times varying all the RF phase values randomly over a range of ±10% and without restricting the phase-modulation profile of the basic elements to be symmetric with respect to the center of the pulse. These calculations were carried out employing a variety of computer systems including a unix cluster with 64 processors, incorporating RF field inhomogeneities (±5%) and considering only a limited number of 32 crystallite orientations selected according to the Zaremba-Cheng-Wolfsberg (ZCW) method (Cheng et al. 1973). A Zeeman field strength corresponding to a ^{1}H resonance frequency of 500 MHz and representative spinning speeds of 15 and 20 kHz were employed in this study. All simulations to assess the performance characteristics of the pulse sequences were carried out with the SPINEVOLUTION program (Veshtort and Griffin 2006) considering 168 α and β powder angles selected according to the REPULSION scheme (Bak and Nielsen 1997) and 16 γ angles.

The performance characteristics of the $RN_n^{\nu_S,\nu_k}$ symmetry-based double-quantum dipolar recoupling pulse schemes were evaluated experimentally by the acquisition of ^{15}N–^{13}C chemical shift correlation spectra. The RF pulse sequence shown in Fig. 1a was used for generating correlation data arising from a single magnetisation transfer pathway, e.g., $^{1}H \rightarrow {}^{15}N \rightarrow {}^{13}C$. The sequence Fig. 1b, involving dual receivers, was applied for the simultaneous acquisition of signals arising from both the magnetisation transfer pathways $^{1}H \rightarrow {}^{15}N \rightarrow {}^{13}C$ and $^{1}H \rightarrow {}^{13}C \rightarrow {}^{15}N$. By appropriate phase cycling of the RF pulses (see figure captions), signals arising via unwanted magnetisation transfer pathways, e.g., $^{1}H \rightarrow {}^{13}C \rightarrow {}^{13}C$, are eliminated. The initial transverse $^{15}N/^{13}C$ magnetisation prepared by the first cross-polarisation (CP) step is allowed to evolve under ^{1}H

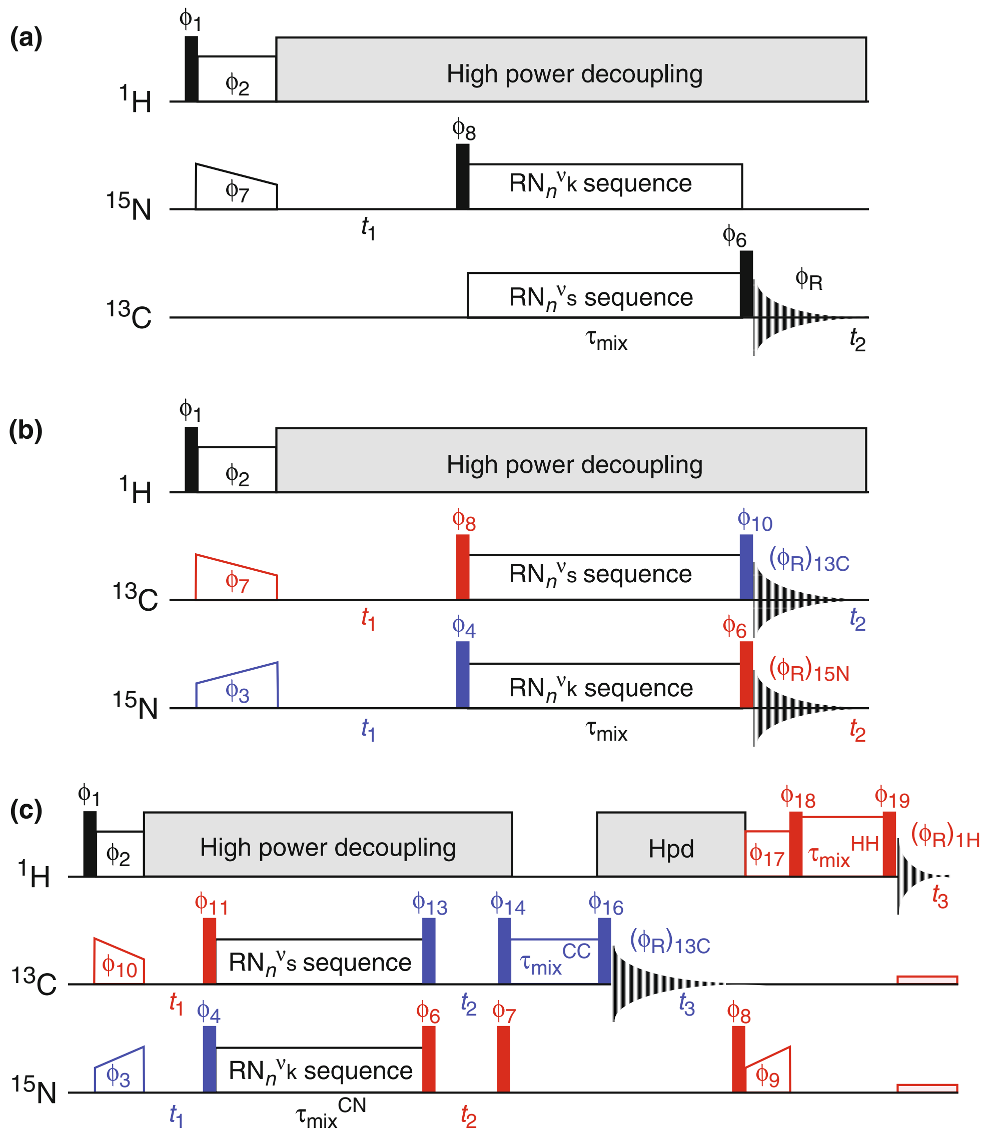

Fig. 1 RF pulse sequences employed for generating chemical shift correlation spectra. The sequences shown in **a** and **b** were applied for obtaining 2D ^{15}N–^{13}C chemical shift correlation spectra via longitudinal magnetisation exchange using either single (**a**) or dual receivers (**b**). The RF pulses shown in *blue* and *red* are applied for generating chemical shift correlation spectra via ^{1}H → ^{15}N → ^{13}C and ^{1}H → ^{13}C → ^{15}N magnetisation transfer pathways, respectively. The RF pulses and the receiver phases were cycled as: ϕ_1 = (y, −y); ϕ_2 = (x); ϕ_3 = (y); ϕ_4 = (2*x, 2*−x); $\phi_6 = \phi_{10}$ = (8*x, 8*y, 8*−x, 8*−y); ϕ_7 = (2*y, 2*−y); ϕ_8 = (4*x, 4*−x); $(\phi_R)_{15N}$ = (x, −x, −x, x, −x, x, x, −x, y, −y, −y, y, −y, y, y, −y, −x, x, x, −x, x, −x, −x, x, −y, y, y, −y, y, −y, −y, y); $(\phi_R)_{13C}$ = (x, −x, −x, x, x, −x, −x, x, y, −y, −y, y, y, −y, −y, y, −x, x, x, −x, −x, x, x, −x, −y, y, y, −y, −y, y, y, −y). The ^{13}C and ^{15}N signals were acquired in t_2 using the corresponding receivers in the two channels. The pulse sequence employed for simultaneous acquisition of 3D NCC (in *blue*) and CN(H)H (in *red*) data sets, respectively, via ^{1}H → ^{15}N → ^{13}C → ^{13}C and ^{1}H → ^{13}C → ^{15}N → ^{1}H magnetisation transfer pathways is shown in **c**. The RF pulses and the receiver phases were cycled as: ϕ_1 = (y, −y); ϕ_2 = (x); ϕ_3 = (y); ϕ_4 = (2*x, 2*−x); ϕ_{13} = (4*x, 4*−x); ϕ_{14} = (8*x, 8*−x); ϕ_{16} = (16*x, 16*−x); $(\phi_R)_{13C}$ = (x, −x, −x, x, −x, x, x, x, −x, −x, x, x, −x, x, −x, −x, x, −x, x, x, −x, x, −x, −x, x, x, −x, −x, x, −x, x, x, −x); ϕ_{10} = (y); ϕ_{11} = (4*x, 4*−x); ϕ_6 = (8*x, 8*−x); ϕ_7 = (x); ϕ_8 = (16*x, 16*−x); ϕ_9 = (y); ϕ_{17} = (x); ϕ_{18} = (y); ϕ_{19} = (32*−y, 32*y); $(\phi_R)_{1H}$ = (x, −x, x, −x, −x, x, −x, x, −x, x, −x, x, x, x, −x, x, −x, −x, x, −x, x, x, −x, x, −x, x, −x, x, −x, −x, x, −x, x, −x, x, −x, x, −x, x, x, −x, x, −x, x, −x, x, −x, −x, x, −x, x, x, −x, x, −x, −x, x, −x, x, −x, x, −x, x, −x, x, x, −x, x, −x). The ^{13}C and ^{1}H signals were acquired in t_3 using the corresponding receivers in the two channels. High power ^{1}H decoupling via SPINAL 64 (Fung et al. 2000; De Paepe et al. 2003) scheme was employed and phase sensitive 2D and 3D spectra were generated by the States procedure (States et al. 1982)

decoupling during the t_1 period and is then flipped to the z-axis by a $\pi/2$ pulse. The longitudinal magnetisation is allowed to evolve under the recoupled ^{13}C–^{15}N dipolar coupling during the mixing period τ_{mix} in the presence of high power ^{1}H decoupling. The ^{13}C/^{15}N magnetisation at the end of τ_{mix} is rotated back to the transverse plane and

detected in t_2. An extension of the sequence Fig. 1b makes it possible to simultaneously acquire 3D NCC and CN(H)H chemical shift correlation data sets of appropriately isotopically labelled biological systems (Fig. 1c). In this scheme, the transverse ^{13}C and ^{15}N magnetisations generated via the two magnetisation transfer pathways mentioned above are allowed to evolve under the isotropic chemical shifts during the t_2 period and then flipped to the z-axis by $\pi/2$ pulses. The ^{13}C longitudinal magnetisation, driven by a broadband homonuclear dipolar recoupling sequence, e.g. RFDR (Bennett et al. 1998), undergoes magnetisation exchange during the mixing period $\tau_{\mathrm{mix}}^{\mathrm{CC}}$ and is then brought back to the transverse plane for direct detection during the t_3 period. After the completion of the acquisition of the ^{13}C FID, the ^{15}N longitudinal magnetisation is brought back to the transverse plane and subjected to a short CP step for transferring the t_1 and t_2 modulated ^{15}N magnetisation to the directly attached proton. The proton magnetisation is then flipped to the z-axis and longitudinal magnetisation exchange mediated by proton–proton dipolar couplings is allowed to take place during the mixing period $\tau_{\mathrm{mix}}^{\mathrm{HH}}$. The proton magnetisation at the end of the mixing period is rotated back to the transverse plane for direct detection during the t_3 period. Phase-sensitive data were generated via standard procedures. Polycrystalline (^{13}C, ^{15}N) labelled samples of L-histidine hydrochloride monohydrate and the CUG triplet repeat expansion RNA $(\mathrm{CUG})_{97}$ (see supplementary material for a schematic representation) were used in the experimental studies carried out on a 500 MHz wide-bore Bruker Avance III solid state NMR spectrometer equipped with 3.2/2.5 mm triple resonance probes with the cooling air kept at a temperature of ~ -50°C. Other details are given in the figure captions.

Results and discussion

Numerical optimisation runs for generating efficient $\mathrm{RN}_n^{\nu_S,\nu_k}$ symmetry-based dual channel RF pulse schemes for γ-encoded broadband ^{15}N–^{13}C dipolar recoupling were carried out at MAS frequencies of 15 and 20 kHz considering representative values for the range of resonance offsets, RF field strengths and CSA parameters in the ^{15}N and ^{13}C channels. In general, it was possible to employ a variety of symmetries for achieving efficient double-quantum dipolar recoupling and, additionally, for each symmetry a variety of phase-modulated basic elements leading to efficient dipolar recoupling could be generated. Using a Mac Pro with 4 cores, typically, generation of symmetry-based dipolar recoupling schemes could be achieved in a short time (<1 h). Other details are given in the figure captions. The simulated performance characteristics of some of the $\mathrm{RN}_n^{\nu_S,\nu_k}$ symmetry-based sequences generated at the MAS frequency of 15 kHz are shown in Fig. 2 along with the optimised RF field-modulation profiles of the basic elements (a1–a4, b1–b4). The optimised profiles (a1–a3, b1–b3) and (a4, b4) were, respectively, obtained considering a resonance offset range of (± 5, ± 5 kHz) and (± 5, ± 1 kHz) for ^{13}C and ^{15}N nuclei. The simulated plots (c1–c4) show the magnitude of the transferred magnetisation (normalised to the maximum transferable signal) on nitrogen starting with z magnetisation on carbon at zero mixing time. Plots given in Fig. 3d1–d4 show, as a function of the resonance offsets of the dipolar coupled nuclei, the magnitude of the transferred magnetisation on nitrogen at τ_{mix} values given in the figure caption. Optimised pulse profiles were first generated considering nominal values for ^{15}N and ^{13}C CSAs (a1, b1; a4, b4). Although such optimised phase-modulation profiles could be obtained using a relatively smaller RF field strength it was seen via numerical simulations that the performance characteristics of such sequences were not satisfactory in the presence of large CSAs. Hence, optimised profiles were generated considering explicitly large CSA values in the numerical calculations (a2, b2; a3, b3). In comparison to the sequence $\mathrm{R24}_9^{-5,-10}$ with the basic R element $\{(\pi/3)_0(5\pi/3)_\pi(\pi/3)_0\}^{s,k}$ (Brinkmann and Levitt 2001), the performance of the numerically optimised symmetry-based sequences is seen to be better. In addition to the above mentioned sequences, dipolar recoupling schemes employing smaller RF field strengths were also generated considering a ^{15}N and ^{13}C resonance offset range of (± 1, ± 1 kHz) (data not shown). Analogous to the plots in Fig. 2, the simulated performance characteristics of some of the $\mathrm{RN}_n^{\nu_S,\nu_k}$ symmetry-based sequences generated at a MAS frequency of 20 kHz are shown in Fig. 3 along with the optimised RF phase-modulation profiles of the basic elements (a1–a3, b1–b3). The phase-modulation profiles shown in (a1, b1) and (a2, b2; a3, b3) were generated, respectively, considering nominal and large CSA values. As expected, the performance of the numerically optimised symmetry-based schemes reported here were in general found to be not affected by minor variations ($\pm 5\%$) in the RF field strength employed. In addition to the symmetries mentioned above, efficient heteronuclear dipolar recoupling could also be achieved with other symmetries and the phase modulation profiles of the corresponding basic R elements are given in the supplementary material. While the recoupling sequences reported here were generated considering a heteronuclear dipolar coupling strength of 1 kHz, it was seen that it is equally possible to generate efficient recoupling sequences considering a smaller dipolar coupling strength. From the numerical simulation results shown in Figs. 2 and 3 it can be seen that it is possible to implement efficient DQ recoupling schemes even at high MAS frequencies using only a moderate

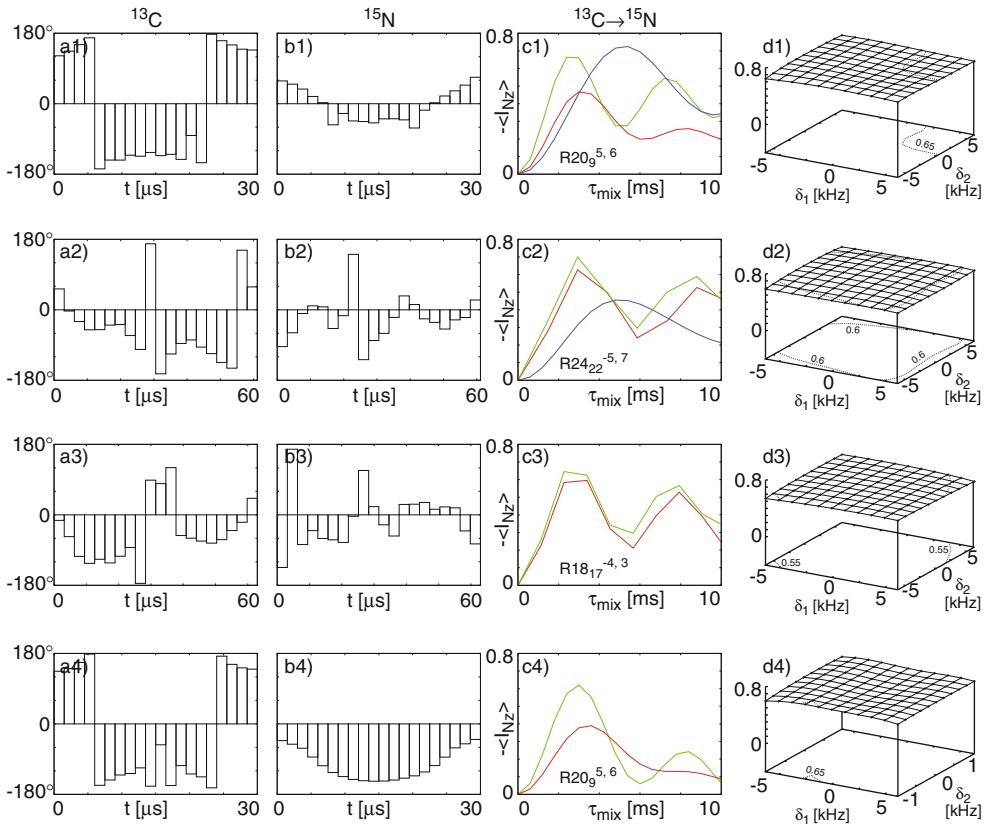

Fig. 2 Phase-modulation profiles (**ai**, **bi**)$_{i=1-4}$ and simulated magnetisation transfer characteristics (**ci**, **di**)$_{i=1-4}$ of the numerically optimised symmetries $R20_9^{5,6}$ (**a1**, **b1**, **c1**, **d1**), $R24_{22}^{-5,7}$ (**a2**, **b2**, **c2**, **d2**), $R18_{17}^{-4,3}$ (**a3**, **b3**, **c3**, **d3**) and $R20_9^{5,6}$ (**a4**, **b4**, **c4**, **d4**). The optimised profiles (**a1**–**a3**, **b1**–**b3**) and (**a4**, **b4**) were, respectively, obtained considering a resonance offset range of (±5, ±5 kHz) and (±5, ±1 kHz) for ^{13}C and ^{15}N nuclei. At a spinning speed of 15 kHz and for a Zeeman field strength corresponding to a ^{1}H resonance frequency of 500 MHz, simulations with these symmetries were carried out, respectively, with R elements of durations 30, 61.1, 63.0, 30 μs, and with ^{13}C and ^{15}N RF field strengths of (35, 35 kHz), (44, 44 kHz), (43, 43 kHz) and (35, 25 kHz) during mixing. The simulated plots (**c1**–**c4**) show the magnitude of the transferred magnetisation (normalised to the maximum transferable signal) on nitrogen starting with z magnetisation on carbon. The simulations were carried out using following chemical shift, scalar and dipolar coupling parameters: plots shown in green: ^{13}C: isotropic shift $\delta_{iso} = 0$ ppm, shift anisotropy $\delta_{aniso} = -19.43$ ppm, asymmetry parameter $\eta = 0.98$, Euler angles $\Omega_{PM} = \{99.4°, 146.0°, 138.9°\}$, ^{15}N: $\delta_{iso} = 0$ ppm, $\delta_{aniso} = 0$ ppm, $\eta = 0$, $\Omega_{PM} = \{0°, 0°, 0°\}$, dipolar coupling $D = 1{,}000$ Hz, $\Omega_{PM} = \{0°, 0°, 0°\}$, J-coupling $J = 6.3$ Hz; plots shown in red: ^{13}C: isotropic shift $\delta_{iso} = 0$ ppm, shift anisotropy $\delta_{aniso} = -76.0$ ppm, asymmetry parameter $\eta = 0.9$, Euler angles $\Omega_{PM} = \{0°, 0°, 94.0°\}$, ^{15}N: $\delta_{iso} = 0$ ppm, $\delta_{aniso} = 99.0$ ppm, $\eta = 0.19$, $\Omega_{PM} = \{-90°, -90°, -17°\}$, dipolar coupling $D = 1{,}000$ Hz, $\Omega_{PM} = \{0°, 0°, 0°\}$, J-coupling $J = 6.3$ Hz. Plots shown in blue were generated employing the sequence $R24_9^{-5,-10}$ with the basic R element $\{(\pi/3)_0(5\pi/3)_\pi(\pi/3)_0\}^{s,k}$ using smaller (**c1**) or larger (**c2**) CSA values, respectively. Plots given in (**d1**–**d4**) show, as a function of the resonance offsets of the dipolar coupled nuclei, the magnitude of the transferred magnetisation on nitrogen at a τ_{mix} of 2.4, 2.9, 2.4, 3.0 ms, starting with z magnetisation on the carbon spin at zero mixing time and using smaller (**d1**, **d4**) or larger (**d2**, **d3**) CSA values, respectively. The RF phase values for the 20 slices of the basic R elements are given in the supplementary material

^{13}C/^{15}N RF field strength of less than 50 kHz by choosing appropriate symmetries.

The performance characteristics of the symmetry-based sequences reported here were first assessed via experimental measurements carried out on a polycrystalline sample of histidine and some of the symmetries were subsequently employed for obtaining ^{15}N–^{13}C chemical shift correlation spectra of the CUG triplet repeat expansion RNA $(CUG)_{97}$. Some representative data generated employing the different RF pulse schemes given in Fig. 1 are presented here and in the supplementary material. Figure 4 shows the 2D ^{15}N–^{13}C chemical shift correlation spectra obtained via longitudinal magnetisation exchange at a spinning speed of 20 kHz (a) and 15 kHz (b, c) using the $R24_{22}^{-5,7}$ (a) and $R18_{17}^{-4,3}$ (b, c) symmetry-based phase-modulated double-quantum dipolar recoupling schemes. The spectra (a) and (b, c) were, respectively, obtained employing the RF pulse schemes given in Fig. 1a and b. While the spectrum (a), collected via the magnetisation transfer pathway $^{1}H \rightarrow {}^{15}N \rightarrow {}^{13}C$, was obtained using a

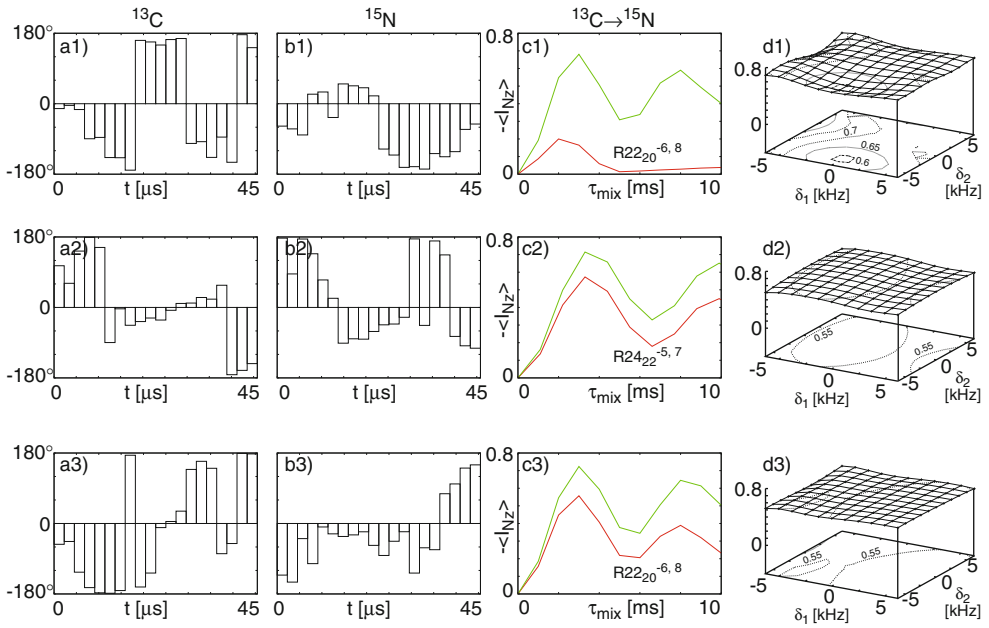

Fig. 3 Phase-modulation profiles (**a**i, **b**i)$_{i=1-3}$ and simulated magnetisation transfer characteristics (**c**i, **d**i)$_{i=1-3}$ of the numerically optimised symmetries $R22_{20}^{-6,8}$ (**a**1, **b**1, **c**1, **d**1), $R24_{22}^{-5,7}$ (**a**2, **b**2, **c**2, **d**2) and $R22_{20}^{-6,8}$ (**a**3, **b**3, **c**3, **d**3). The optimised profiles (**a**1–**a**3, **b**1–**b**3) were obtained considering a resonance offset range of (±5, ±5 kHz) for ^{13}C and ^{15}N nuclei and nominal (**d**1) or larger (**d**2, **d**3) CSA values, respectively (see Fig. 2). At a spinning speed of 20 kHz and for a Zeeman field strength corresponding to a ^{1}H resonance frequency of 500 MHz, simulations with these symmetries were carried out, respectively, with *R* elements of durations 45.5, 45.8, 45.5 μs, and with ^{13}C and ^{15}N RF field strengths of (33, 33 kHz), (44, 44 kHz) and (45, 45 kHz) during mixing. The simulated plots (**c**1–**c**3) show the magnitude of the transferred magnetisation (normalised to the maximum transferable signal) on nitrogen starting with *z* magnetisation on carbon. The simulations were carried out using chemical shift, scalar and dipolar coupling parameters as in Fig. 2. Plots given in (**d**1–**d**3) show, as a function of the resonance offsets of the dipolar coupled nuclei, the magnitude of the transferred magnetisation on nitrogen at a τ_{mix} of 3.0, 3.3, 3.0 ms, starting with *z* magnetisation on the carbon spin at zero mixing time and using smaller (**d**1) or larger (**d**2, **d**3) CSA values, respectively. The RF phase values for the 20 slices of the basic *R* elements are given in the supplementary material

CP contact time of 2 ms, the spectra (b) and (c) were collected simultaneously employing a short CP contact time of 300 μs. A few representative cross-sections at the positions indicated in spectra (b) and (c) are also given to indicate spectral quality. The corresponding spectral cross-sections taken from data collected under similar experimental conditions using the symmetry $R24_9^{-5,-10}$ with the composite pulse based *R* elements $\{(\pi/3)_0(5\pi/3)_\pi(\pi/3)_0\}^{s,k}$ are also given for comparison. In agreement with the numerical simulations, the symmetry-based sequence with the numerically optimised basic *R* element performs better. The crosspeak intensities seen in the heteronuclear correlation spectra are not only related to the efficacy of the dipolar recoupling scheme but also to the magnitude of ^{15}N/^{13}C magnetisation at $\tau_{mix} = 0$. The large CP contact time employed in generating the spectrum in Fig. 4a leads to ^{15}N → ^{13}C crosspeaks with measurable signal intensities even for ^{15}N nuclei without any attached protons, e.g. N1, N9 → C1′; G_{N7} → $G_{C5,C8}$. All the ^{15}N → ^{13}C correlation peaks leading to the characteristic connectivity patterns of the different nucleotides can be clearly seen in this spectrum. The crosspeak intensities observed in ^{15}N–^{13}C chemical shift correlation spectra can be very weak in situations where there is a significant reduction in the transverse magnetisation generated at the end of long CP contact times. Under these circumstances, it may be advantageous to employ short CP contact times and dual receivers to generate ^{15}N–^{13}C chemical shift correlation spectra simultaneously via both the magnetisation transfer pathways ^{1}H → ^{15}N → ^{13}C and ^{1}H → ^{13}C → ^{15}N. In the spectra shown in Fig. 4b, c collected with a short CP contact time, the crosspeaks essentially arise, respectively, from ^{15}N and ^{13}C nuclei with directly attached protons. Although many of the CN correlation peaks present in spectrum Fig. 4a are missing in spectrum 4b, many of these missing correlation peaks, e.g. C1′ → N1, N9, could be seen with measurable signal intensities in the spectrum shown in Fig. 4c acquired with ^{15}N detection. The possibility to simultaneously acquire signals arising from the two magnetisation transfer pathways mentioned above can also be exploited to simultaneously acquire 3D NCC and CNH data sets, as shown in Fig. 5. The 2D spectral projections (zoomed plot) given in Fig. 5 were generated from 3D CNH ($\tau_{mix}^{HH} = 0$) and NCC data sets. These were

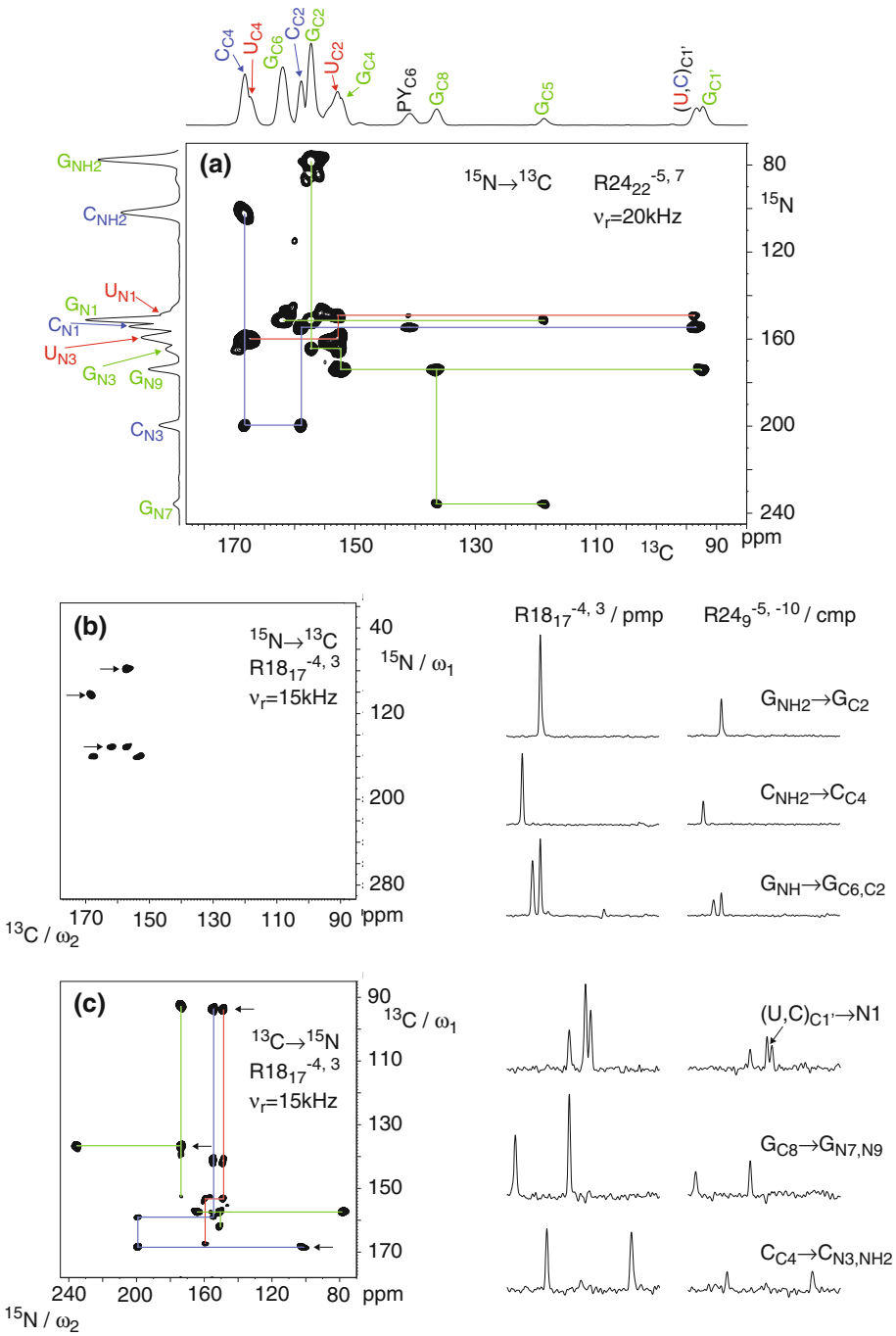

Fig. 4 2D ^{15}N–^{13}C chemical shift correlation spectra of $(CUG)_{97}$. The spectrum **a** was collected at a spinning speed of 20 kHz via the magnetisation transfer pathway ^{1}H → ^{15}N → ^{13}C employing the RF pulse sequence given in Fig. 1a, a CP contact time of 2 ms, the R24$_{22}^{-5,7}$ symmetry with the corresponding numerically optimised *R* elements (pmp) given in Fig. 3a2 and b2, a mixing time of 1.1 ms, ^{13}C and ^{15}N RF field strength of 44 kHz, 96 transients per t_1 increment, 96 t_1 increments, a spectral width in the indirect dimension of 12,000 Hz and a recycle time of 2.5 s. The RF carriers were kept approximately at the center of the spectral regions. The spectra **b** and **c** were collected simultaneously at a spinning speed of 15 kHz, employing the RF pulse sequence given in Fig. 1b, a short CP contact time of 300 μs, a mixing time of 1.13 ms, the R18$_{17}^{-4,3}$ symmetry with the corresponding numerically optimised *R* elements given in Fig. 2a3 and b3, ^{13}C and ^{15}N RF field strength of 43 kHz, 48 transients per t_1 increment, 128 t_1 increments, a spectral width in the indirect dimension of 14,000 Hz and recycle time of 2 s. The RF carriers were kept approximately at the center of the spectral regions. A few representative cross-sections taken at the positions indicated in spectra **b** and **c** are also given. The corresponding spectral cross-sections taken from data collected under similar experimental conditions using the symmetry R24$_9^{-5,-10}$ with a composite pulse based *R* element (cmp) (see text) are also given for comparison. The spectrum using the symmetry R24$_9^{-5,-10}$ was collected employing a mixing time of 1.2 ms and with ^{13}C and ^{15}N RF field strengths of 47 kHz

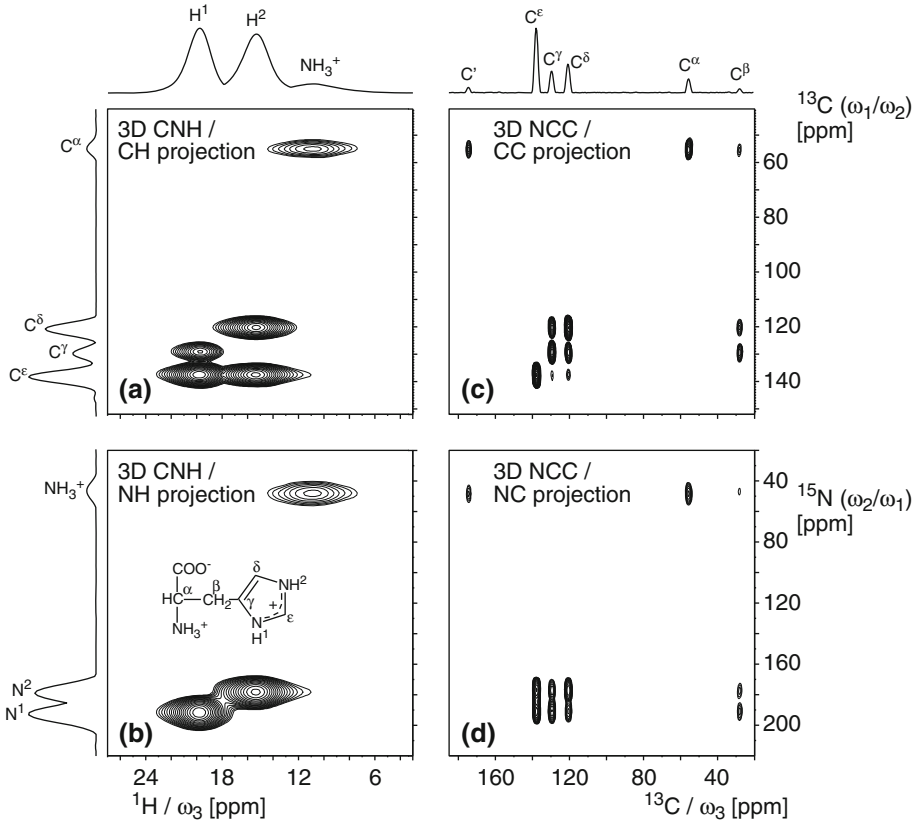

Fig. 5 2D spectral projections (zoomed plot) generated from 3D CNH ($\tau_{mix}^{HH} = 0$) and NCC data sets that were acquired simultaneously employing the RF pulse sequence given in Fig. 1c, a spinning speed of 20 kHz, a CP contact time of 300 μs, a uniformly (^{13}C, ^{15}N) labelled sample of L-histidine hydrochloride monohydrate, 32 transients per t_1 increment, 32 t_1 and t_2 increments, ^{15}N and ^{13}C spectral widths in the indirect dimension of 20,000 Hz and a recycle time of 2 s. The ^{15}N and ^{13}C RF carriers were kept at 120 ppm. The ^{15}N–^{13}C mixing ($\tau_{mix}^{CN} = 1.1$ ms) was achieved via the $R24_{22}^{-5,7}$ symmetry-based phase-modulated double-quantum dipolar recoupling scheme, as in Fig. 4a. ^{13}C–^{13}C dipolar recoupling ($\tau_{mix}^{CC} = 2.4$ ms) was carried out in the absence of ^{1}H decoupling via the RFDR sequence employing broadband phase-modulated inversion pulses of 12 μs duration applied with an RF field strength of 100 kHz and the *xy*-16 phasing scheme (Herbst et al. 2009a)

collected via the RF pulse sequence given in Fig. 1c at a spinning speed of 20 kHz employing L-histidine hydrochloride monohydrate. As in Fig. 4a, the ^{15}N–^{13}C mixing was achieved via the $R24_{22}^{-5,7}$ symmetry-based phase-modulated double-quantum dipolar recoupling scheme. ^{13}C–^{13}C dipolar recoupling during the mixing period τ_{mix}^{CC} was carried out in the absence of ^{1}H decoupling via the RFDR sequence. Broadband phase-modulated inversion pulses of 12 μs duration applied with an RF field strength of 100 kHz and the *xy*-16 phasing scheme (Herbst et al. 2009a) were employed. Other details are given in the figure caption. As expected, the short mixing time of $\tau_{mix}^{CN} = 1.1$ ms leads to crosspeaks originating only from directly coupled ^{15}N–^{13}C spin pairs. While relayed magnetisation transfers arising from ^{13}C–^{13}C dipolar recoupling can be clearly seen in the 3D NCC spectral projections, the CH and NH projections from the 3D CNH spectrum show only crosspeaks arising from directly bonded ^{13}C–^{15}N–^{1}H spin networks due to $\tau_{mix}^{HH} = 0$. However, the availability of appropriately ^{13}C, ^{15}N and ^{2}H labelled protein samples would make it possible to obtain information about ^{1}H–^{1}H spatial proximities via longitudinal magnetisation exchange mediated by proton–proton dipolar couplings during the mixing period τ_{mix}^{HH} (Zhou et al. 2007b). As in our recent study (Herbst et al. 2008) the RF pulse sequence given in Fig. 1c can be easily modified to take different spectral width requirements in the ^{15}N and ^{13}C channels into account. The 3D data sets were collected in this study via the conventional approach of incrementing t_1 and t_2 step-by-step. However, it is possible to achieve further reduction of the data acquisition time by incrementing t_1 and t_2 simultaneously and generate the 3D spectra via the projection-reconstruction procedure (Kupce and Freeman 2004).

The results presented here clearly demonstrate that it is possible to implement efficient $RN_n^{\nu_S,\nu_k}$ type of symmetry-based dual channel RF pulse schemes for γ-encoded broadband ^{15}N–^{13}C dipolar recoupling at high MAS

frequencies. The symmetry-based approach provides a large number of inequivalent $RN_n^{\nu_S,\nu_k}$ sequences. It is seen that it is possible to generate efficient dipolar recoupling sequences by choosing appropriate symmetries, for which phase-modulated basic *R* elements of required durations can be generated employing the available/applicable RF power. The fact that there exist a large number of possibilities for implementing dipolar recoupling sequences via the symmetry-based approach has to be considered as an opportunity to be exploited rather than a headache to be dealt with. While in the present study the *R* elements were implemented as a sandwich of a small number of short pulses of equal duration with each pulse characterised by a RF phase value, it is conceivable that in situations where basic elements of long duration are required, e.g. in the design of band-selective recoupling sequences, it may be advantageous to employ a finite Fourier series representation of the phase-modulation profile to minimise the computational time required. It has to be mentioned that it is necessary to carry out the numerical optimisation procedure considering a large number of appropriate symmetries for generating the best possible dipolar recoupling sequence with the lowest possible applied RF field strength. Such an investigation has not been attempted here and is beyond the scope of the present study. In this study dealing with broadband dipolar recoupling we have used phase-modulated *R* elements of constant amplitude. However, it is possible to employ amplitude and phase-modulated *R* elements that may be required, for example, in the design of efficient band-selective recoupling sequences (Nielsen et al. 2009). The method outlined here can also be extended to the design of recoupling sequences that can be implemented without the simultaneous application of high power ^{1}H decoupling (see supplementary material). In the context of the systems studied and the Zeeman field strength employed, the ^{15}N–^{13}C DQ dipolar recoupling sequences reported here were mostly developed by considering a resonance offset range of ±5 kHz for the ^{13}C and ^{15}N nuclei. Initial studies indicate (see supplementary material) that it is equally possible to generate recoupling sequences to satisfy different bandwidth requirements in the ^{13}C and ^{15}N channels, e.g. for sequential backbone ^{15}N and ^{13}C resonance assignments in proteins. The numerical approach presented here can be adapted for generating REDOR-type heteronuclear dipolar recoupling schemes that can also be used for CSA recoupling with suppression of chemical shift terms and homonuclear dipolar couplings. Such studies are currently in progress in our laboratory.

Acknowledgments This study has been funded in part by a grant from the Deutsche Forschungsgemeinschaft (GO474/6-1). The FLI is a member of the Science Association 'Gottfried Wilhelm Leibniz' (WGL) and is financially supported by the Federal Government of Germany and the State of Thuringia.

References

Bak M, Nielsen NC (1997) REPULSION, a novel approach to efficient powder averaging in solid state NMR. J Magn Reson 125:132–139

Baldus M (2002) Correlation experiments for assignment and structure elucidation of immobilized polypeptides under magic angle spinning. Prog Nucl Magn Reson Spectrosc 41:1–47

Bennett AE, Griffin RG, Vega S (1994) Recoupling of homo- and heteronuclear dipolar interactions in rotating solids. NMR basic principles and progress, vol 33. Springer, Berlin, pp 1–77

Bennett AE, Rienstra CM, Griffiths JM, Zhen W, Lansbury PT, Griffin RG (1998) Homonuclear radio frequency-driven recoupling in rotating solids. J Chem Phys 108:9463–9479

Brinkmann A, Levitt M (2001) Symmetry principles in the nuclear magnetic resonance of spinning solids: heteronuclear recoupling by generalized Hartmann-Hahn sequences. J Chem Phys 115: 357–384

Castellani F, van Rossum BJ, Diehl A, Rehbein K, Oschkinat H (2003) Determination of solid-state NMR structures of proteins by means of three-dimensional 15N–13C-13C dipolar correlation spectroscopy and chemical shift analysis. Biochemistry 42:11476–11483

Cheng VB, Suzukawa HH, Wolfsberg M (1973) Investigations of a nonrandom numerical method for multidimensional integration. J Chem Phys 59:3992–3999

De Paepe G, Lesage A, Emsley L (2003) The performance of phase modulated heteronuclear dipolar decoupling schemes in fast magic-angle-spinning nuclear magnetic resonance experiments. J Chem Phys 119:4833–4841

Detken A, Hardy EH, Ernst M, Kainosho M, Kawakami T, Aimoto S, Meier BH (2001) Methods for sequential resonance assignment in solid, uniformly ^{13}C, ^{15}N labelled peptides: quantification and application to antamanide. J Biomol NMR 20:203–221

Dusold S, Sebald A (2000) Dipolar recoupling under magic-angle spinning conditions. Annu Rep NMR Spectrosc 41:185–264

Forrest S (1993) Genetic algorithms—principles of natural-selection applied to computation. Science 261:872–878

Freeman R, Wu XL (1987) Design of magnetic resonance experiments by genetic evolution. J Magn Reson 75:184–189

Frericks HL, Zhou DH, Yap LL, Gennis RB, Rienstra CM (2006) Magic-angle spinning solid-state NMR of a 144 kDa membrane protein complex: *E. coli* cytochrome bo_3 oxidase. J Biomol NMR 36:55–71

Fung BM, Khitrin AK, Ermolaev K (2000) An improved broadband decoupling sequence for liquid crystals and solids. J Magn Reson 142:97–101

Goldberg DE (1989) Genetic algorithms in search, optimization and machine learning. Addison-Wesley, Massachusetts

Griffin RG (1998) Dipolar recoupling in MAS spectra of biological solids. Nature Struct Biol 5:508–512

Hansen JO, Kehlet C, Bjerring M, Vosegaard T, Glaser SJ, Khaneja N, Nielsen NC (2007) Optimal control based design of composite dipolar recoupling experiments by analogy to single-spin inversion pulses. Chem Phys Lett 447:154–161

Haupt RL, Haupt SE (2004) Practical genetic algorithms. Wiley, Hoboken

Herbst C, Riedel K, Ihle Y, Leppert J, Ohlenschläger O, Görlach M, Ramachandran R (2008) MAS solid state NMR of RNAs with multiple receivers. J Biomol NMR 41:121–125

Herbst C, Herbst J, Kirschstein A, Leppert J, Ohlenschläger O, Görlach M, Ramachandran R (2009a) Design of high-power, broadband 180° pulses and mixing sequences for fast MAS solid state chemical shift correlation NMR spectroscopy. J Biomol NMR 43:51–61

Herbst C, Herbst J, Kirschstein A, Leppert J, Ohlenschläger O, Görlach M, Ramachandran R (2009b) Recoupling and decoupling of nuclear spin interactions at high MAS frequencies: numerical design of CN_n^v symmetry-based RF pulse schemes. J Biomol NMR 44:175–184

Herbst C, Herbst J, Leppert J, Ohlenschläger O, Görlach M, Ramachandran R (2009c) Numerical design of RN_n^v symmetry-based RF pulse schemes for recoupling and decoupling of nuclear spin interactions at high MAS frequencies. J Biomol NMR 44:235–244

Hong M (1999) Resonance assignment of $^{13}C/^{15}N$ labeled solid proteins by two- and three-dimensional magic-angle-spinning NMR. J Biomol NMR 15:1–14

Judson R (1997) Genetic algorithms and their use in chemistry. In: Lipkowitz KB, Boyd DB (eds) Reviews in computational chemistry, vol 10. VCH, New York, pp 1–73

Kehlet C, Bjerring M, Sivertsen AC, Kristensen T, Enghild JJ, Glaser SJ, Khaneja N, Nielsen NC (2007) Optimal control based NCO and NCA experiments for spectral assignment in biological solid-state NMR spectroscopy. J Magn Reson 188:216

Kupce E, Freeman R (2004) Projection-reconstruction technique for speeding up multidimensional NMR spectroscopy. J Am Chem Soc 126:6429–6440

Levitt MH (2002) Symmetry-based pulse sequences in magic-angle spinning solid-state NMR. In: Grant DM, Harris RK (eds) Encyclopedia of nuclear magnetic resonance. Wiley, Chichester

Nielsen AB, Bjerring M, Nielsen JT, Nielsen NC (2009) Symmetry-based dipolar recoupling by optimal control: band-selective experiments for assignment of solid-state NMR spectra of proteins. J Chem Phys 131:025101

Pauli J, Baldus M, van Rossum B, de Groot H, Oschkinat H (2001) Backbone and side-chain ^{13}C and ^{15}N signal assignments of the α-spectrin SH3 domain by magic angle spinning solid-state NMR at 17.6 Tesla. ChemBioChem 2:272–281

Riedel K, Leppert J, Ohlenschläger O, Görlach M, Ramachandran R (2005) TEDOR with adiabatic inversion pulses: resonance assignments of $^{13}C/^{15}N$ labelled RNAs. J Biomol NMR 31:49–57

Rienstra CM, Hohwy M, Hong M, Griffin R (2000) 2D and 3D 15N–13C-13C chemical shift correlation spectroscopy of solids: assignment of MAS spectra of peptides. J Am Chem Soc 122: 10979–10990

Siemer AB, Ritter C, Steinmetz MO, Ernst M, Riek R, Meier BH (2006) ^{13}C, ^{15}N resonance assignment of parts of the HET-s prion protein in its amyloid form. J Biomol NMR 34:75–87

States DJ, Haberkorn RA, Ruben DJ (1982) A two-dimensional nuclear overhauser experiment with pure absorption phase in four quadrants. J Magn Reson 48:286–292

Sun BQ, Rienstra CM, Costa PR, Williamson JR, Griffin RG (1997) 3D 15N–13C–13C chemical shift correlation spectroscopy in rotating solids. J Am Chem Soc 119:8540–8546

van Rossum BJ, Castellani F, Pauli J, Rehbein K, Hollander J, de Groot HJM, Oschkinat H (2003) Assignment of amide proton signals by combined evaluation of HN, NN and HNCA MAS-NMR correlation spectra. J Biomol NMR 25:217–223

Veshtort M, Griffin RG (2006) SPINEVOLUTION: a powerful tool for the simulation of solid and liquid state NMR experiments. J Magn Reson 178:248–282

Wall M (1996) GAlib: A C++ Library of genetic algorithm components, version 2.4.7. http://lancet.mit.edu/ga/

Wu XL, Freeman R (1989) Darwin's ideas applied to magnetic resonance. The marriage broker. J Magn Reson 85:414–420

Xu P, Wu XL, Freeman R (1992) User-friendly selective pulses. J Magn Reson 99:308–322

Zhou DH, Shah G, Cormos M, Franks WT, Mullen C, Sandoz D, Rienstra CM (2007a) Proton-detected solid-state NMR spectroscopy of fully protonated proteins at 40 kHz magic-angle spinning. J Am Chem Soc 129:11791–11801

Zhou DH, Shea JJ, Nieuwkoop AJ, Franks WT, Wylie BJ, Mullen C, Sandoz D, Rienstra CM (2007b) Solid-state protein-structure determination with proton-detected triple-resonance 3D magic-angle-spinning NMR spectroscopy. Angew Chem Int Ed 46: 8380–8383